CrossMark

Preparation and characterization of TiO$_2$-coated hollow glass microsphere and its flame-retardant property in thermoplastic polyurethane

Hongzhi Wang[1] · Chuanmei Jiao[1] · Li Zhao[1] · Xilei Chen[1]

Abstract In this paper, a novel and efficient halogen-free flame retardant, HGM@TiO$_2$, was synthesized by coating hollow glass microspheres (HGM) with TiO$_2$. The flame-retardant and smoke suppression properties of HGM@TiO$_2$ in thermoplastic polyurethane (TPU) have been investigated using several techniques including cone calorimeter test (CCT), smoke density test (SDT), thermogravimetric analysis (TGA) and fourier infrared, respectively. The CCT results showed that HGM@TiO$_2$ could greatly improve the flame-retardant properties of TPU composites. The peak heat release rate of the sample with 0.5 wt% HGM@TiO$_2$ (405 kW m^{-2}) was reduced by 64% compared with the sample with the same loading HGM (1117 kW m^{-2}), and the structure of char residue layer of TPU composites was obviously changed. The SDT results showed that HGM@TiO$_2$ could effectively decrease the amount of smoke production in the test. Furthermore, the TGA results indicated that HGM@TiO$_2$ could decrease the initial decomposition temperature and improve the thermal stability of TPU. And the FTIR results revealed that HGM@TiO$_2$ could promote the composites to release inflammable gas such as CO$_2$ earlier to suppress the combustion. According to this study, there may be some new methods to obtain flame-retardant polymer with low loading level.

Keywords Hollow glass microspheres · Coating · TiO$_2$ · Thermoplastic polyurethane · Flame retardant

✉ Xilei Chen
   xilei_chen@foxmail.com

[1] College of Environment and Safety Engineering, Qingdao University of Science and Technology, Qingdao 266042, Shandong, People's Republic of China

Introduction

In recent years, thermoplastic polyurethane (TPU) has been widely used in coatings, films, automotive and infrastructure cables, etc. [1–4]. However, high fire risks associated with TPU, including dense smoke generation, high heat and toxic gases release, have greatly limited its broad applications. As a consequence, the study on how to improve the flame-retardant properties of TPU has attracted more and more attentions. Traditionally, flame retardants containing the halogen [5] will be harmful to people in the process of application, and the demands for halogen-free flame retardants have become more and more important due to the healthy and environmental concerns [6–8].

Intumescent flame retardant, as an environmental friendly flame retardant, has been widely used in the TPU composites [9]. The effect is good, but there are still some disadvantages. Such as the amount of intumescent flame retardant is usually relatively large, which will have a great influence on mechanical properties [10]. Inorganic nano-materials and nano-composite (montmorillonite, clay and nano-ZnO) are also used as flame retardants being added into polymer materials [11–13] and have a good flame-retardant effect [14–17]. But the nano-materials are easy to agglomerate, leading to the particle size too large to disperse uniformly, and the effective controlling of nanoparticle agglomerates is not easy.

Hollow glass microspheres (HGM) have attracted considerable interest in the past few decades because of its excellent physical, such as well-defined morphology, uniform size, strong filling ability, low density, and large surface area, small and well-distributed internal stress in products [18, 19]. HGM were often used to reinforce polymer for its high compression strength and good fluidity [20]. In our previous work, it has been found HGM could

be used as a synergistic agent to improve the flame-retardant efficiency and smoke suppression effect in TPU composites based on APP [20]. HGM have the characteristic of low density and the migration feature of HGM onto the surface of the sample when the composites are in the melt stage, so it could be used as a barrier from the flame zone to the underlying materials, restrained the flammable gases to the flame zone. In addition, TiO_2 also has many excellent characteristics, such as high thermal stability. As a flame retardant, it will migrate onto the polymer surface after the matrix melted. Then, TiO_2 can blend with carbon residue to increase the intensity of the char layer [21]. Combining HGM and TiO_2, there may be good flame-retardant effect in polymer. HGM may be used as effective flame retardants for the polymer with high charring yield property with TiO_2. Currently, researchers on HGM coated with TiO_2 are mainly forced on the field of photocatalysis [22]. And no work has been reported to coat HGM with TiO_2 in flame-retardant field.

In this paper, HGM@TiO_2, as a novel and efficient halogen-free flame retardant, was successfully synthesized by modifying HGM with TiO_2, and characterized by SEM–EDS and XPS, respectively. Then, the flame-retardant, smoke suppression and thermal stability properties of TPU/HGM@TiO_2 composites were intensively investigated using SDT, CCT and TG–IR, respectively.

Experimental

Materials

Hollow glass microsphere (HGM) was produced by the PQ Corporation (grade 5020, with particle size of 5–115 μm, medium particle of 55 μm and density of 0.2 g cm^{-3}). $Ti(SO_4)_2$ was produced by the Tianjin Guangfu Fine Chemical Research Institute. Commercial TPU (9380A) was produced by Bayer, German. The basic properties of TPU are as follows, density: 1.110 g cm^{-3} (ISO1183); hardness: 82A (ISO868); tensile strength: 40 MPa (ISO527-1,-3); and elongation at break: 500% (ISO527-1,-3).

Sample preparation

Synthesis of HGM@TiO$_2$

Firstly, HGM was rinsed with pure water for 5 min and cleaned with 10% NaOH in ultrasonic cleaner for about 30 min. After that, HGM was washed and filtered with pure water four times and then dried in a vacuum oven at 80 °C for 2 h. Maintaining the temperature at 80 °C, the ethanol (150 mL), water (100 mL) and HGM (8 g) were added to

the flask. At the same time, 20 mL 20% $Ti(SO_4)_2$ solution and 10% NaOH solution were added to the flask slowly, maintaining a pH of 3–6, and the mixed solution was continuously stirred at 80 °C for another 5 h. The upper layer of the HGM@$Ti(OH)_4$ was separated, filtered and rinsed three times with ethanol. The crude product was dried in a vacuum oven at 80 °C for 6 h to obtain the crude products. Then, the products were calcined in a vacuum furnace at 500 °C for 2.0 h, to obtain the HGM@TiO_2 (Scheme 1).

Preparation of TPU/HGM@TiO$_2$ composites

The TPU pellets were dried at 80 °C for 4 h. A certain amount of TPU was melted in the mixer at 175 °C. Then, a certain amount of HGM or HGM@TiO_2 was added into the mixer. Later, the samples were hot-pressed at about 180 °C under 10 MPa for 20 min into sheets of suitable thickness for analysis. Formulations of flame-retardant TPU composites: TPU/HGM with 99.5 wt% TPU and 0.5 wt% HGM; TPU/HGM@TiO_2 with 99.5 wt% TPU and 0.5 wt% HGM@TiO_2.

Measurements

Scanning electron microscopy (SEM)

Scanning electron microscopy (SEM) was performed using a Hitachi X650 scanning electron microscope.

Cone calorimeter test (CCT)

The cone calorimeter (Stanton Redcroft, UK) tests were performed according to ISO 5660 standard procedures. Each specimen of dimensions $100 \times 100 \times 3$ mm^3 was wrapped in aluminum foil and exposed horizontally to an external heat flux of 35 kW m^{-2}.
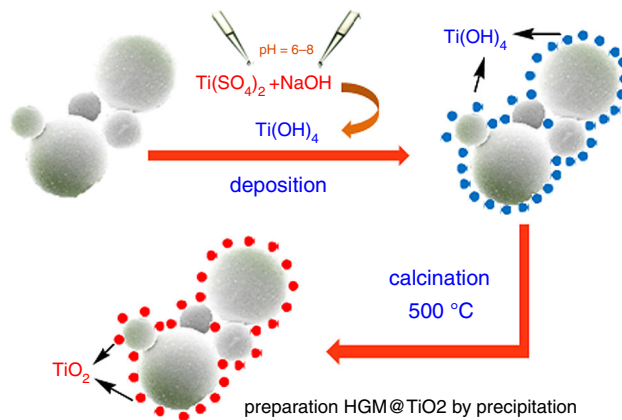
Scheme 1 Schematic illustration of synthesis of HGM@TiO_2

Smoke density test (SDT)

A smoke density test machine JQMY-2 (Jianqiao Co, China) was used to measure the smoke characteristics according to ISO 5659-2 (2006). Each specimen of dimensions $75 \times 75 \times 2.5$ mm^3 was wrapped in aluminum foil and exposed horizontally to an external heat flux of 25 kW m^{-2}.

Thermogravimetric analysis/infrared spectrometry (TG–IR)

Thermogravimetric analysis (TGA) of the sample was performed using a DT-50 (Setaram, France) instrument. About 10.0 mg of sample was put in an alumina crucible and heated from ambient temperature to 700 °C. The heating rates were set as 20 °C min^{-1} (nitrogen atmosphere, flow rate of 60 mL min^{-1}). Thermogravimetric analysis/infrared spectrometry (TG–IR) of the cured sample was performed using a DT-50 (Shimadzu, Japan) instrument that was interfaced to a Varian 2000 FTIR spectrometer.

Results and discussion

Characterization of HGM@TiO$_2$

Figure 1 showed the photographs of HGM and HGM@TiO$_2$ in SEM. It could be seen that there was obvious distinction between HGM and HGM@TiO$_2$. For HGM (HGM-A, HGM-A′), there was nothing on the surface of it. But for HGM@TiO$_2$ (HGM@TiO$_2$-B, HGM@TiO$_2$-B′), some particles were on the surface with dense and ultrafine, indicating that the particles may be TiO$_2$ particles. The analytical results of the chemical elements from the material of the HGM@TiO$_2$ were that of 9.2% Ti, as shown in Fig. 2. The XRD patterns of the HGM, HGM@TiO$_2$ are shown in Fig. 3. It could be seen that a number of XRD peaks for the anatase TiO$_2$ attest the
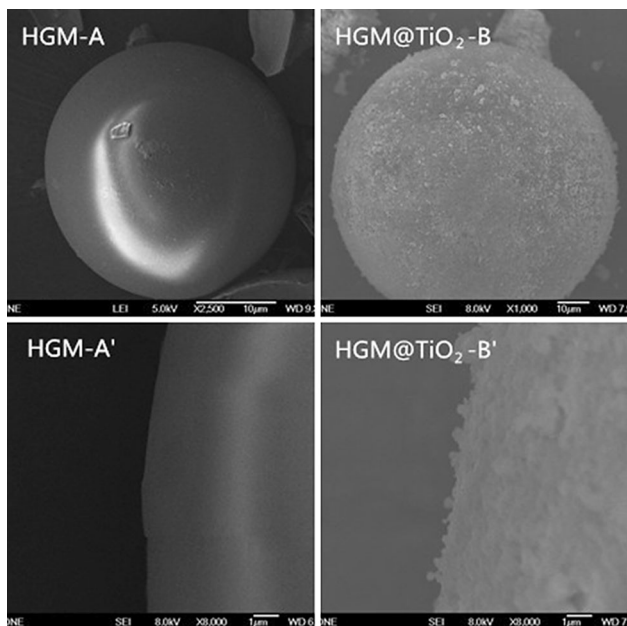

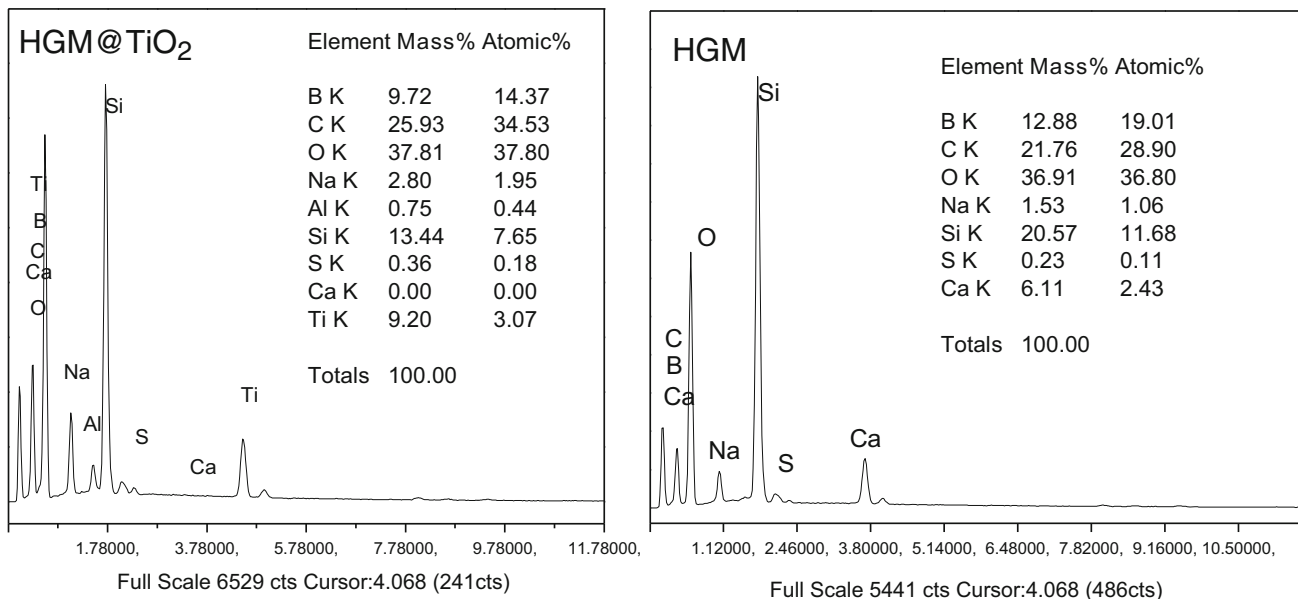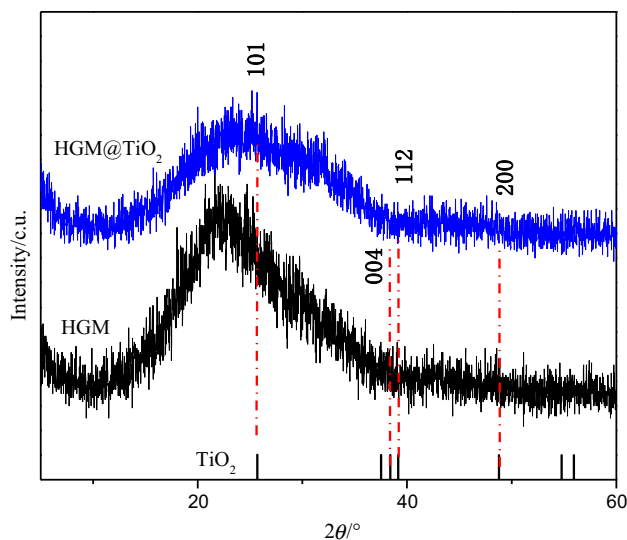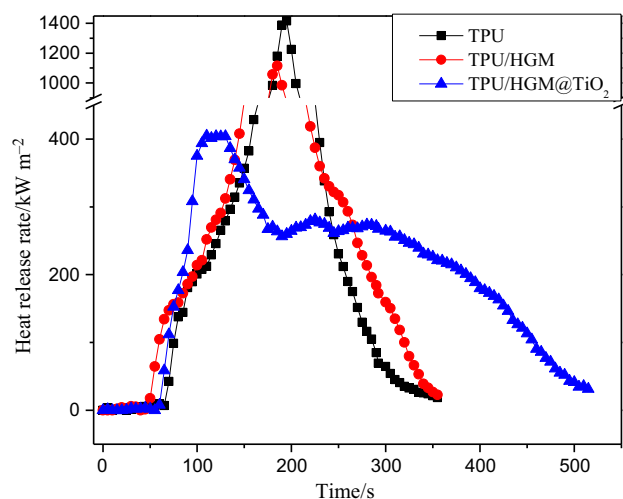**Fig. 1** SEM image of the outer surface of HGM/HGM-TiO$_2$

Fig. 2 EDS results of HGM/HGM@TiO$_2$

Fig. 3 XRD results of HGM/HGM@TiO$_2$

Fig. 5 Total heat release curves of flame-retardant TPU composites at flux of 35 kW m^{-2}

Fig. 4 Heat release rate curves of flame-retardant TPU composites at a flux of 35 kW m^{-2}
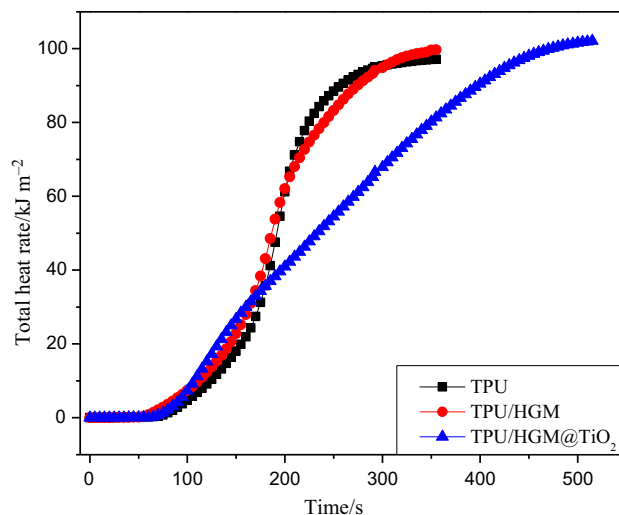

Fig. 6 Mass loss curves of flame-retardant TPU composites at a flux of 35 kW m^{-2}

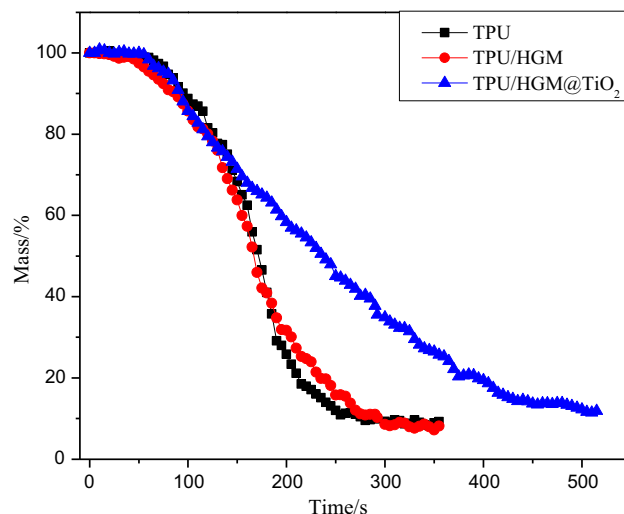good crystallinity after the coated reaction. So the modification has been tested to be feasible.

Cone calorimeter test

Heat release rate (HRR)

The heat release rate (HRR) curves for the samples are shown in Fig. 4. It was easy to see that TPU was a relatively flammable polymeric material, and a sharp peak HRR (PHRR) (1429 kW m^{-2}) was obtained at 195 s. The PHRR value of TPU/HGM was 1117 kW m^{-2} at 185 s, and the PHRR value of TPU/HGM@TiO$_2$ was 405 kW m^{-2} at 110 s. The PHRR value of TPU/HGM@TiO$_2$ decreased significantly compared with TPU or TPU/HGM, which

meant that the flame-retardant effect of TPU composites with HGM@TiO$_2$ was better than that of HGM to reduce the HRR when the loading of flame retardant was 0.5 wt%. The above phenomenon could be explained by the compact char residue forming on the surface of sample [23]. TPU could be softened by heat, and then, both HGM and HGM@TiO$_2$ could migrate progressively onto the surface of the sample and change the structure of char residue layer preventing heat and mass transfer between underlying materials and flame zone, thus reducing the HRR. However, for the samples with HGM@TiO$_2$, TiO$_2$ on the surface of HGM can further promote the char formation and change the structure of char residue.

In addition, the ignition time (IT) of composite became shorter after HGM or HGM@TiO$_2$ being added into TPU.

The reason may be that HGM or HGM@TiO$_2$ migrated onto the surface of the sample to promote the decomposition of TPU at short time. It also could be seen that TPU or TPU/HGM had a single peak, which could be easily explained by the sample gradually burning. It was interesting that the HRR curve of TPU/HGM@TiO$_2$ sample had two peaks. The first peak was identified as the development of the intumescing char, which could protect samples; the second peak was due to the fact that the protective carbon layer gradually degraded as the sample was continuously exposed to the heat from cone.

Total heat release (THR)

Figure 5 presented the THR curves of all the samples. The slope of the THR curve was assumed to be representative of flame spread [24]. It could be seen the THR of the samples of TPU or TPU/HGM was higher than that of TPU/HGM@TiO$_2$ at the end of the combustion. The flame spread of TPU or TPU/HGM was obviously faster than that of TPU/HGM@TiO$_2$ between 50 and 250 s. It was seen that the slope of the sample with HGM@TiO$_2$ remained remarkably low, which was conducive to prevent the spread of fire. The results showed that the flame spread of TPU or TPU/HGM was quickly in the earlier stage. In the case of TPU/HGM@TiO$_2$, the heat insulation of HGM@TiO$_2$ could be obtained during the combustion process, which resulted in the low THR. Furthermore, there was no apparent effect when an equal amount of HGM was added into TPU compared with pure TPU; there was the lowest THR for TPU/HGM@TiO$_2$ because of the TiO$_2$ on the surface of HGM.
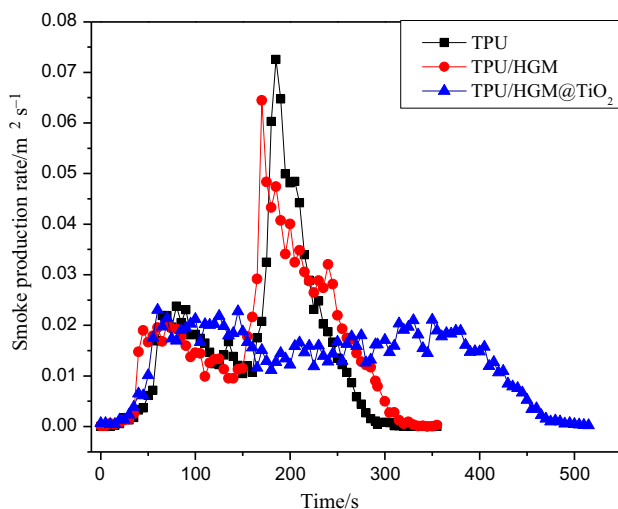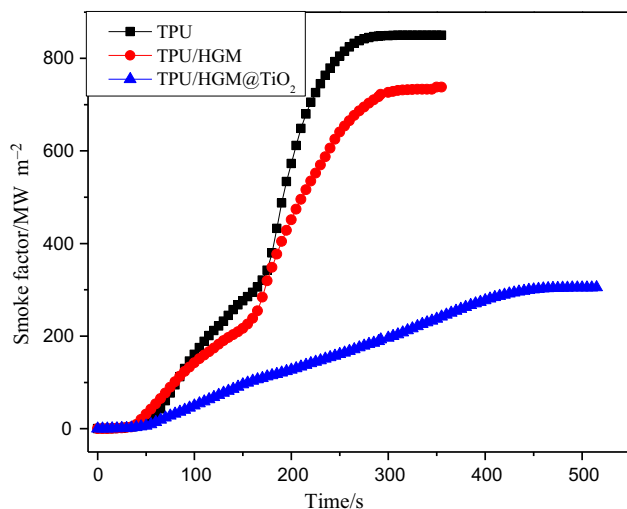

Fig. 7 Smoke production rate curves of flame-retardant TPU composites at flux of 35 kW m^{-2}
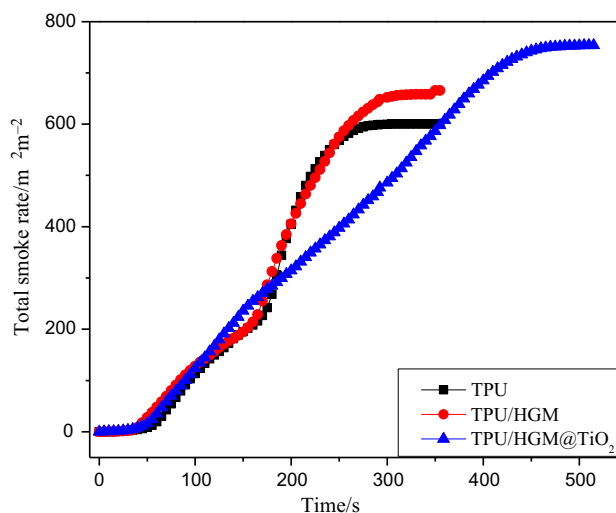
Fig. 8 Total smoke release curves of flame-retardant TPU composites at flux of 35 kW m^{-2}

Mass

Figure 6 presented the mass curves of the samples. It could be seen that TPU/HGM had the highest mass loss before 130 s, followed by TPU/HGM@TiO$_2$ and TPU, respectively. This result could be used to illustrate why the ignition time of TPU/HGM sample was shorter than those of TPU and TPU/HGM@TiO$_2$. Furthermore, the mass loss of TPU/HGM was larger than those of TPU and TPU/HGM@TiO$_2$ during the combustion process in range of 130–180 s, and the mass loss of TPU was larger than those of TPU/HGM and TPU/HGM@TiO$_2$ during the combustion process after 180 s. This meant that the protective carbon layer had been generated for TPU/HGM at about 180 s. High mass loss meant there was much larger amount of volatile compounds formed. Combining the results from Fig. 5, the volatiles compounds were mainly flammable gases. The reason for the high mass loss for TPU/HGM and TPU/HGM@TiO$_2$ in early stage (50–130 s) was that it could promote the pyrolytic reaction; once the protective char carbon was formed, HGM or HGM@TiO$_2$ would play positive effects role on flame retardant. However, the mass loss rate of TPU/HGM@TiO$_2$ was significantly lower than TPU or TPU/HGM at later stage. This can be explained that HGM@TiO$_2$ could change the structure of char residue layer. On the one hand, HGM@TiO$_2$ could make the char residue compact, and on the other hand, HGM@TiO$_2$ could migrate onto the surface of the samples during the heat process, showing good barrier effect for heat and mass transferring, Further explanation was that TiO$_2$ on the surface of HGM could promote the carbonization of TPU to form char residue layer. Then, the mass loss values of sample TPU/HGM@TiO$_2$ reduced to the same low levels as TPU/HGM or TPU, due to the fact that the char residue

**Fig. 9** Smoke factor curves of flame-retardant TPU composites at flux of 35 kW m^{-2}

was unstable and could be oxidized in the conditions with high temperature and oxygen.

Smoke production rate (SPR)

Smoke performance of flame-retardant material is a very important parameter in fire safety fields [25]. The incomplete combustion of flame-retardant composite systems can be seen in the smoke production rate [26]. The smoke production rate (SPR) curves of TPU composites are given in Fig. 7. Compared with the peak SPR values of TPU (0.072 m^2 s^{-1}) and TPU/HGM (0.064 m^2 s^{-1}), the peak SPR value of TPU/HGM@TiO$_2$ was 0.023 m^2 s^{-1}, which was the lowest one among all samples. The peak SPR value decreased greatly with the addition of TPU/HGM@TiO$_2$, and the smoke suppression effect of HGM@TiO$_2$ was more obvious than that of HGM. It could be explained as follows: HGM@TiO$_2$ can migrate onto the surface, which can improve the stability of the char residue layer, protecting the inner matrix, and reduce the amount of smoke-forming materials in the gas phase during combustion.

Total smoke release (TSR)

Figure 8 presented the total smoke release (TSR) curves of the samples. It could be seen that the TSR of TPU/HGM@TiO$_2$ was slightly higher than those of TPU and TPU/HGM before 180 s. This illustrated that HGM could change the structure of char residue from TPU/HGM in the combustion process, which results in less smoke particulates released. After 300 s, the TSR of TPU and TPU/HGM was greatly higher than that of TPU/HGM@TiO$_2$ until the end of combustion. TPU/HGM@TiO$_2$ had a low TSR
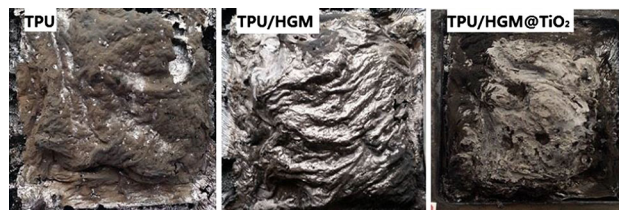
Fig. 10 Photographs of flame-retardant TPU composites after CCT

value compared with TPU/HGM during 180–350 s, which was attributed to the fact that the rupture of char residue layer in the combustion process. The ultimate TSR value of sample TPU was 602 m^2 m^{-2} (TPU/HGM was 659 m^2 m^{-2}; TPU/HGM@TiO$_2$ was 754 m^2 m^{-2}). The TSR value from TPU/HGM@TiO$_2$ was higher than that of TPU or TPU/HGM at the end of CCT, which was attributed to formed compact char layer residue lead to the internal material of smoldering with the continuous heating by cone calorimeter. In fire, materials smolder, less heat release, but produce a lot of smoke [27].

Smoke factor (SF)

Figure 9 gave the smoke factor (SF) curves of all samples. SF is the production of HRR and TSR. SF values described the hazards of fire by the aspect of heat and smoke [28]. The peak SF values for all samples were 851, 735 and 304 kW m^{-2}, respectively. It could be seen that the addition of a certain amount of HGM could reduce the fire hazards of TPU composites. And, HGM@TiO$_2$ could further decrease the fire hazard of TPU composites, including heat (Fig. 5) and smoke (Fig. 8). So, HGM@TiO$_2$ could be used as effective flame-retardant and smoke suppression agent for TPU.

Photographs of char residue

Figure 10 showed the photographs of char residues after CCT. A carbonaceous char formed during expansion, which could act as a thermal shield between the flame zone and the substrate, preventing heat from penetrating. It could be seen that there were many cracks and holes on the surface of carbon layer from TPU sample. This structure cannot effectively bind combustible gas and smoke particulates from the underlying materials, resulting in high HRR and SPR. For TPU/HGM, there were many bigger micro-holes, which cannot release flammable gases into flame zone, but it could play the role of heat insulation resulting high HRR. This result cannot be used to illustrate the HRR and SPR results. However, the mass results in Fig. 6 could be combined with the structure of char residue

Fig. 11 SEM images of the (TPU-A ×200) and (TPU-A′ ×1000) magnification views of char residue of TPU composites after CCT. (TPU/HGM-B ×200) and TPU/HGM-B′ ×1000) magnification views of the TPU/HGM composites. (TPU/HGM@TiO$_2$-C ×200) and (TPU/HGM@TiO$_2$-C′ ×1000) magnification views of the TPU/HGM@TiO$_2$ composites
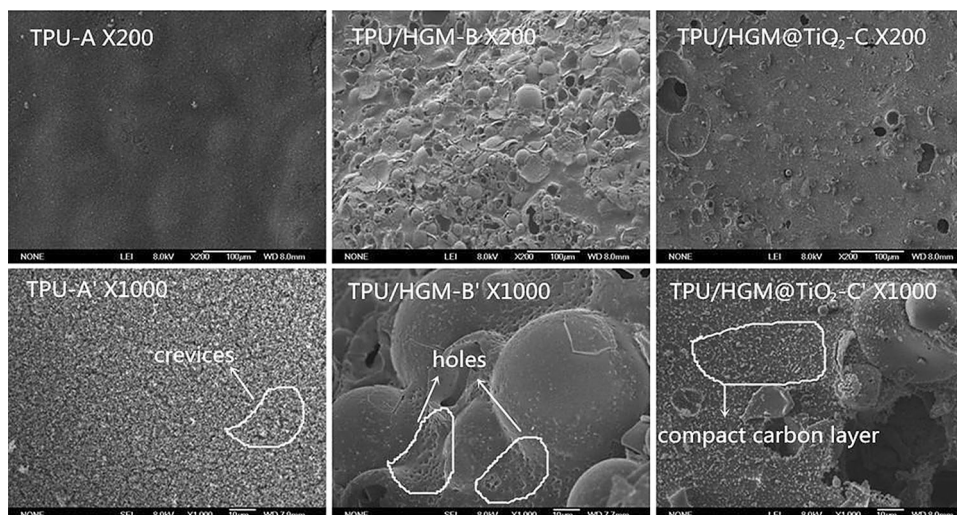
after CCT. From Fig. 6, it had been concluded that TiO$_2$ could promote carbonization of TPU between 180 and 300 s. At the same time range, the low HRR and SPR were also gotten. It could speculate that there was much dense char residue layer formed on the surface of sample. But, the char residue was unstable, which can be oxidized with high temperature and oxygen.

Photograph of the char layer

The morphologies and structures of char residue of TPU, TPU/HGM and TPU/HGM@TiO$_2$ after CCT were examined by SEM and EDS. Typical images were shown in Figs. 11 and 12. In the low magnification (200× TPU-A, TPU/HGM-B, TPU/HGM@TiO$_2$-C) views, numerous particles with micrometer-sized diameter were appeared on below the surface. The high magnified images (1000× TPU-A′, TPU/HGM-B′, TPU/HGM@TiO$_2$-C′) displayed the different surface morphologies between TPU/HGM and TPU/HGM@TiO$_2$. For TPU/HGM@TiO$_2$-C′, the char residue image showed a compact appearance and smooth surface. Compared with TPU/HGM@TiO$_2$-C′, the TPU/HGM-B′ sample surface appeared a significant uplift phenomenon, the result of extensional fracturing of the char residue surface structure due to longitudinal compression warping deformation. The char residue of TPU/HGM@TiO$_2$ has better thickness and mechanical strength compared with TPU/HGM. In addition, there were many holes on the surface of HGM (TPU/HGM-B′) sample, and there were many crevices on the surface of TPU (TPU-A′) sample. In contrast, the char residue of HGM@TiO$_2$ (TPU/HGM@TiO$_2$-C′) showed a compact appearance and smooth surface. Holes and crevices were nearly not existed in the char residue of TPU/HGM@TiO$_2$. This could be explained that HGM@TiO$_2$ could help to promote charring
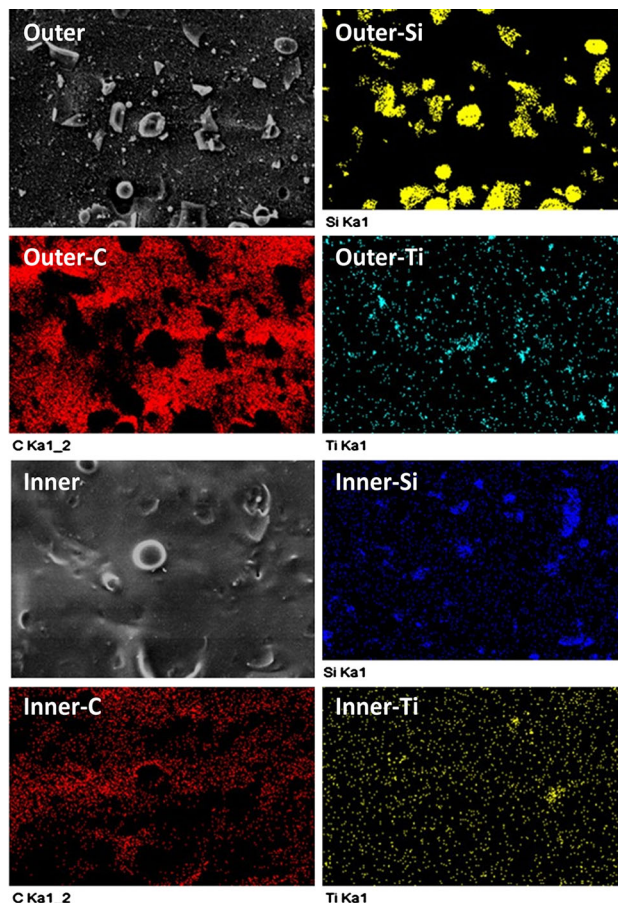
Fig. 12 The EDS images from char residues of outer (outer-C, outer-Si, outer-Ti) and inner (inner-C, inner-Si, inner-Ti) surface of TPU/HGM@TiO$_2$ composites after CCT

change the structure of carbon layer and form compact carbon layer.

EDS images showed that the distribution of both Ti and Si atom had a strong consistency. As seen from Fig. 12

Table 1 The content of elements of outer/inner surface by EDS test

Element	Outer surface		Inner surface	
	Mass%	Atomic%	Mass%	Atomic%
B K	9.38	10.87	8.17	9.15
C K	73.71	76.90	85.66	86.33
O K	14.44	11.31	5.79	4.38
Al K	0.16	0.07	0.03	0.01
Si K	1.30	0.58	0.21	0.09
Ti K	1.02	0.27	0.14	0.04
Totals	100.00		100.00	

[inner (Si, C, Ti), outer (Si, C, Ti)], the Ti and Si atom distribution density and central tendency of the inner/outer surface were represented through the EDS images. It was easy to find that both the inner surface and the outer surface have the distribution of Si atom and Ti atom. However, the density is different. The EDS results of char residues were given in Table 1. It could be clearly seen that the Si atom content on outer surface (1.30 wt%) was higher than that of inner surface (0.21 wt%); the Ti atom content on outer surface (1.02 wt%) was also higher than that of inner surface (0.14 wt%). The results confirmed that HGM or HGM@TiO$_2$ could migrate progressively onto the surface of the sample when burnt.

Fire performance index (FPI) and fire growth index (FGI)

In order to judge the fire hazard of composites, the fire performance index (FPI) and the fire growth index (FGI) are calculated after CCT. The FPI is defined as the ratio of time from ignition to PHRR, and the FGI is defined as the ratio of peak HRR to time to PHRR [29, 30]. From Fig. 13, it could be seen that the FPI values increased and the FGI values decreased for TPU/HGM@TiO$_2$ compared with pure TPU. The results showed that the FPI values of sample TPU/HGM@TiO$_2$ (0.121 m^2 s kW^{-1}) were improved by three times compared with TPU/HGM

(0.042 m^2 s kW^{-1}); the FGI values of sample TPU/HGM@TiO$_2$ (3.67 kW m^2 s^{-1}) were reduced by two times compared with pure TPU/HGM (7.25 kW m^2 s^{-1}). It can be concluded that HGM@TiO$_2$ could extend the time of reach crashing and then reduce the risk of fire, which indicates the sample with TPU/HGM@TiO$_2$ have good flame retardancy.

Thermogravimetric analysis (TGA)

Figure 14a showed the TGA curves for all samples. The initial decomposition temperatures of TPU, TPU/HGM and TPU/HGM@TiO$_2$ were 330, 303 and 295 °C, respectively. It could be seen that HGM and HGM@TiO$_2$ could promote the thermal degradation of TPU at low temperature. When the temperature was raised to 508 °C, the remaining char residues of TPU, TPU/HGM and TPU/HGM@TiO$_2$ were 11.9, 9.3 and 41.9%, respectively. The temperature was raised to 700 °C, and the remaining char residues were 10.3, 8.5 and 8.9%, respectively. There was a turning point in the TPU/HGM (365 °C, 37.6%) and TPU/HGM@TiO$_2$ (435 °C, 41.9%) curves. Compared with the sample with HGM, the turning point temperature of the composite with HGM@TiO$_2$ significantly improved.

The DTG curves were given in Fig. 14b, and the degradation reaction of composites could be divided into three stages. First stage, the water was evaporated at about 258, 185 and 210 °C, respectively. Second stage, the peak temperature of TPU, TPU/HGM and TPU/HGM@TiO$_2$ decomposition was 361, 343 and 642 °C, respectively. And it could be seen that HGM could improve the formation of char residue during combustion and accelerate the composite system to crack. However, it did not bring significant mass loss when HGM@TiO$_2$ was added into the composites. Last stage, the peak represented the decomposition of soft domains. The peak decomposition temperatures of TPU, TPU/HGM and TPU/HGM@TiO$_2$ were 433, 457 and 404 °C, respectively. The mass loss rate for TPU (the peak value was −21% min^{-1}) was significantly higher than that for TPU/HGM (−5.5% min^{-1}) and TPU/HGM@TiO$_2$

**Fig. 13** Fire performance index for flame-retardant TPU composites at flux of 35 kW m^{-2}
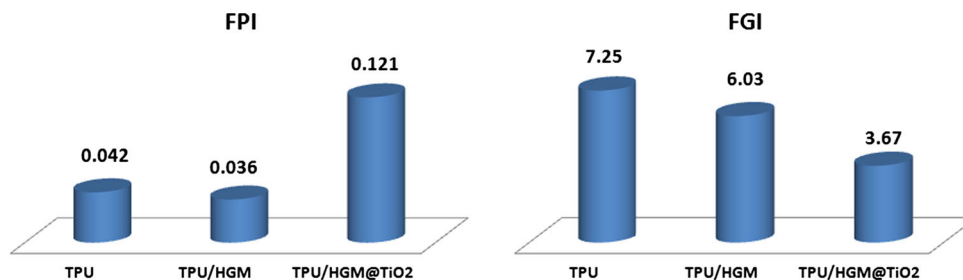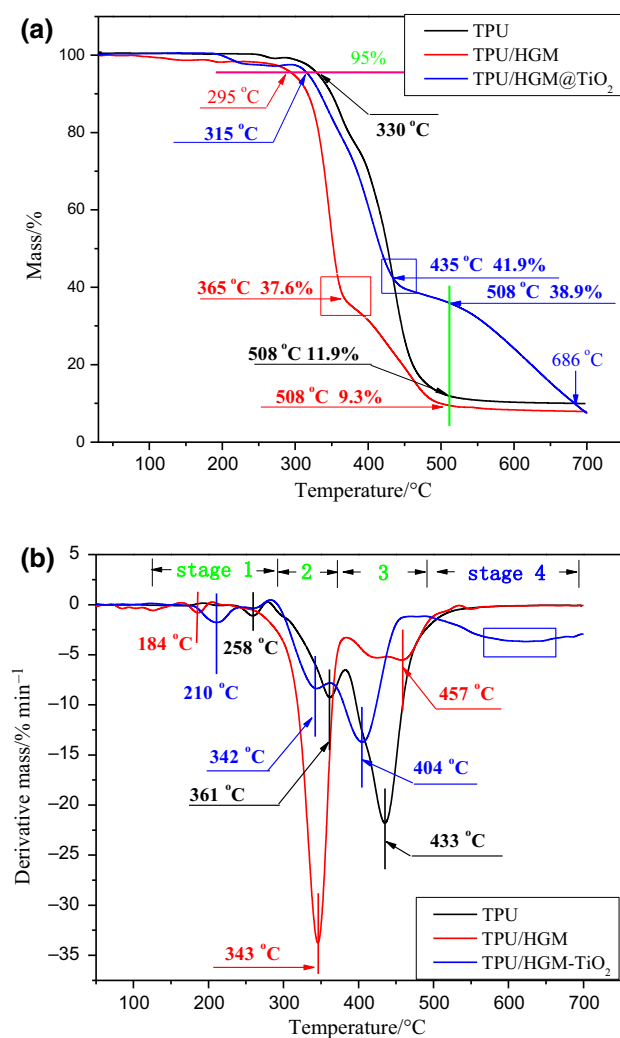
Fig. 14 TG (**a**) /DTG (**b**) curves of flame-retardant TPU composites at a constant heating rate of 10 K min^{-1}

(-13.0% min^{-1}). Both the samples TPU/HGM@TiO₂ and TPU have same residual because less decomposition rate at the stage 2. The difference between the sample of TPU/HGM@TiO₂ and TPU at the stage 3 with composite decomposition is, first, the TPU/HGM@TiO₂ decomposition time for arrival of the peak value earlier than TPU; second, the peak value of TPU/HGM@TiO₂ decomposition rate lower than TPU. It was worthy noted that a broad peak (stage 4) appeared on the curve of TPU/HGM@TiO₂. This meant that the composite was not decomposition completely; it was very obvious effect for TPU/HGM@TiO₂. In conclusion, the time to arrive the peak value for TPU/HGM@TiO₂ was earlier than TPU because of the peak accompanied by formation of char layer; however, the time of forming char layer for TPU/HGM was earlier than pure TPU. In stage 2, compared with the DTG results of HGM, the peak DTG temperature of TPU/

HGM@TiO₂ and maximum mass loss were higher. The mass loss of sample TPU/HGM was mainly focused on the stage 2 due to the formation of low char layer efficiency. By contrast, the mass loss of sample TPU/HGM@TiO₂ was mainly focused on the stage 3. For such cases, we explain from two respects. First, the heating methods of the two instruments are different (CCT use side heating and TGA use full-circumferential heating). Second, the size of sample was different. Focused by radiation heat in samples surface external, part of the heat to be reflected back, due to the HGM, has been migrated to the surface. The samples were heated by full-circumferential; the upper HGM cannot play the effectiveness of the insulation. Furthermore, large sample size was easier to form char layer. In conclusion, HGM@TiO₂ could promote TPU thermal decomposition in the early stage and slow down the rate of TPU thermal decomposition in the last stage.

The volatilized products formed during the thermal degradation of the TPU composites were characterized by TG–IR technique and are shown in Fig. 15a–c, respectively. It was obviously noted the peaks around 3230–3550, 2800–3150, 2250–2400, 1700–1850, 1250–1500 and 950–1150 cm^{-1} [31]. Some of the volatilized decomposition products of the TPU were unambiguously identified by characteristic strong FTIR signals, such as H_2O (3230–3550 cm^{-1}), CO_2 (2300–2400 cm^{-1}), CO (2250–2300 cm^{-1}), carboxylic acid (1700–1850 cm^{-1}) and aliphatic hydrocarbons (2800–3150, 1250–1500 and 950–1150 cm^{-1}). In the process of pyrolysis, the main products of the thermal decomposition of TPU were compounds containing H_2O, CO_2, CO, carboxylic acid, and aliphatic hydrocarbons, etc. The pyrolysis processes of these three samples are significantly different according to Fig. 15a–c. In the case of TPU, it decomposed drastically with lots of pyrolysis products, and at last no product released that the composites pyrolyzed completely. The generated trend of CO_2 is shown in Fig. 16. There were two maximum intensity temperatures of CO_2 from TPU/HGM, which were at 450 and 700 °C, respectively. In addition, there were three maximum intensity temperatures of CO_2 from TPU/HGM@TiO₂, which were at 380 and 680 °C, respectively. Also, the initial formation temperature of CO_2 from TPU/HGM@TiO₂ was much lower than that of TPU/HGM. This can be illustrated by the TiO₂ catalyzing polyol from depolymerization of polyurethane to form water. Then, the water can react with isocyanate from depolymerization of polyurethane, generating CO_2. The reason for the second maximum intensity temperatures of TPU/HGM and TPU/HGM@TiO₂ was the self-polymerization among isocyanates from depolymerization of polyurethane to form CO_2, chain segment crosslink and then reduce the formation of combustible gases. At

Fig. 15 3D-FTIR spectra of gas products for TPU (**a**), TPU/HGM (**b**) and TPU/HGM@TiO$_2$ (**c**) at different temperatures
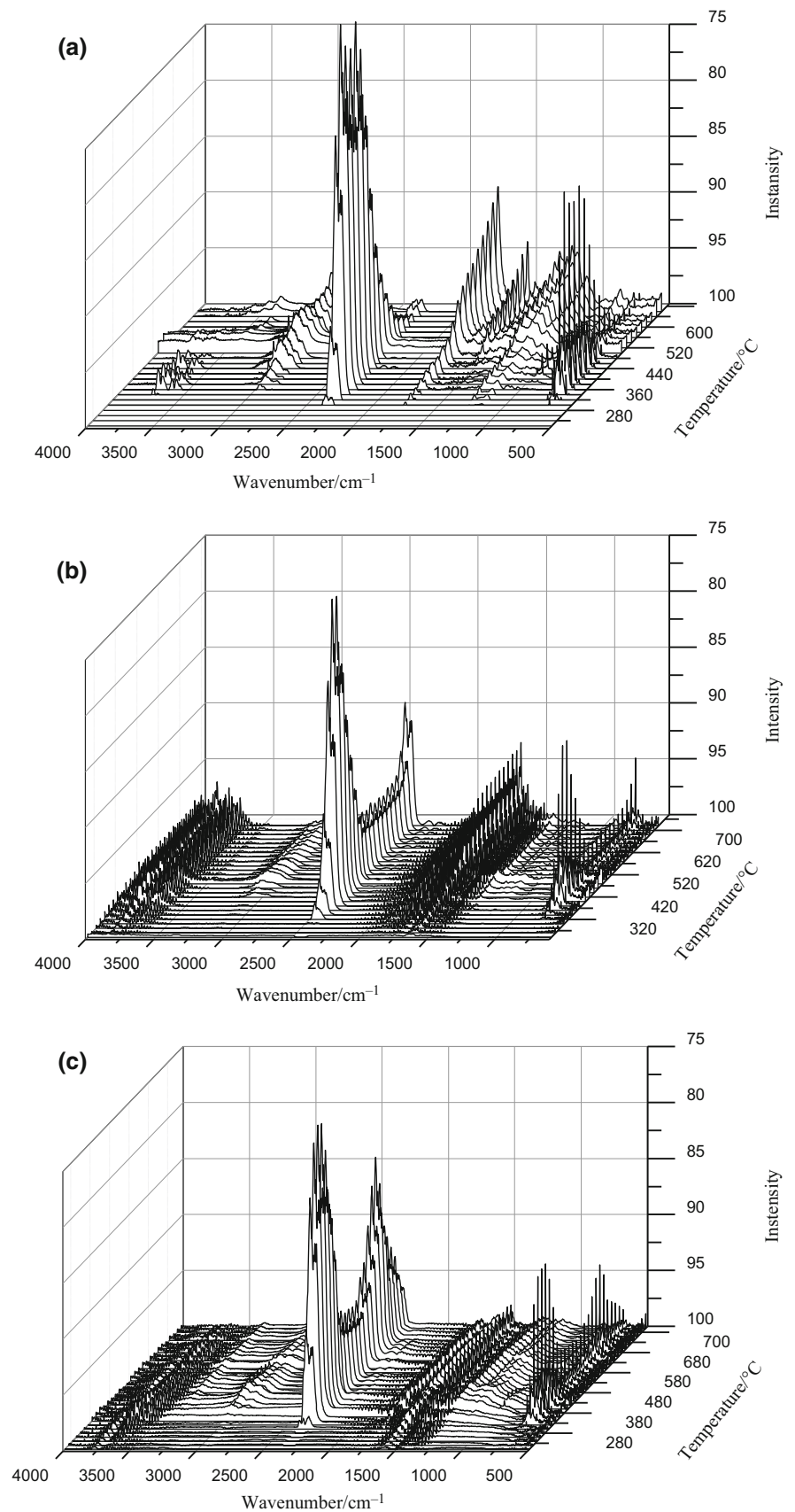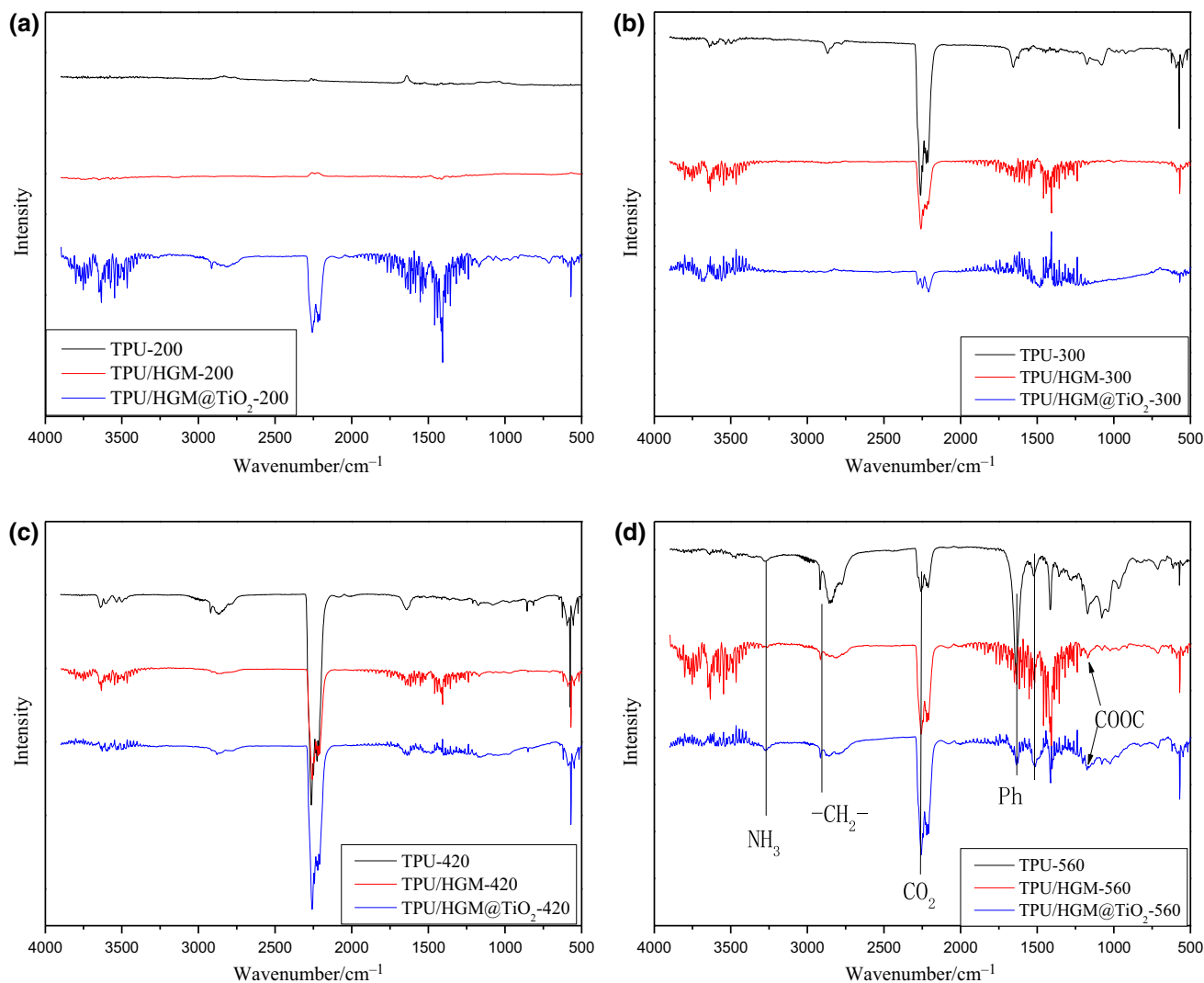
Fig. 16 FTIR spectra of volatilized products during thermal degradation of TPU composites

intermediate stage, the HGM@TiO$_2$ and the char residue played a role in effective making stability and protective.

Figure 16 showed that FTIR spectra obtained at the maximum evolution rates [200 (a), 300 (b), 420 (c) and 560 °C (d)] during the thermal decomposition of TPU, TPU/HGM and TPU/HGM@TiO$_2$, respectively. From Fig. 16a, it could be clearly seen that the peak appeared at 2360 cm^{-1} (CO$_2$), this showed the sample of TPU/HGM@TiO$_2$ has released CO$_2$ at 200 °C. The non-flammable gases (CO$_2$, H$_2$O) released from samples of TPU/HGM@TiO$_2$ can dilute the combustible gases in the gas phase to play the role of flame-retardant efficiency. For Fig. 16b, the peak appears at 2863 cm^{-1} (–CH$_2$–/–CH$_3$–), this showed only the sample of TPU has released hydrocarbons at 300 °C. For Fig. 16c, the peak of all the sample curves is similar, the only difference is the intensity of peaks. The combustion gas content at evolved gaseous

products of TPU was higher than that TPU/HGM or TPU/HGM@TiO$_2$. For Fig. 16d, the sample of TPU had completely burnt out; at the same temperature the TPU/HGM@TiO$_2$ still had residual.

Conclusions

The XRD, SEM and EDS results showed that a novel and efficient halogen-free composite flame-retardant HGM@TiO$_2$ has been synthesized. During the combustion process, HGM@TiO$_2$ can migrate to the surface and promote the formation of carbon layer. The HGM@TiO$_2$ can also greatly reduce the HRR, THR and SPR values, suppress the formation of flammable gases and promote the formation of CO$_2$, promotion of matrix crosslinks, achieving good fire-retardant effect.

References

1. Bocz K, Bárány T, Toldy A, Bodzay B, Csontos I, Madi K, Marosi G. Self-extinguishing polypropylene with a mass fraction of 9% intumescent additive—a new physical way for enhancing the fire retardant efficiency. Polym Degrad Stab. 2013;98:79–86.

2. Shi L, Li Z, Xie B, Wang J, Tian C, Yang M. Flame retardancy of different-sized expandable graphite particles for high-density rigid polyurethane foams. Polym Int. 2006;55:862–71.

3. Deodhar S, Shanmuganathan K, Fan Q, Wilkie C, Costache M, Dembsey N, Patra P. Calcium carbonate and ammonium polyphosphate-based flame retardant composition for polypropylene. J Appl Polym Sci. 2011;120:1866–73.

4. Yang W, Lin Q. Research and application of thermoplastic polyurethane elastomer (TPU). Plast Manuf. 2015;5:70–7.

5. Qian Y, Wei P, Jiang P, Li Z, Yan Y, Liu J. Preparation of a novel PEG composite with halogen-free flame retardant supporting matrix for thermal energy storage application. Appl Energy. 2013;106:321–7.

6. Li H, Ning N, Zhang L, Wang Y, Liang W, Tian M. Different flame retardancy effects and mechanisms of aluminium phosphinate in PPO, TPU and PP. Polym Degrad Stab. 2014;105:86–95.

7. Lu S, Hamerton I. Recent developments in the chemistry of halogen-free flame retardant polymers. Prog Polym Sci. 2002;27:1661–712.

8. Jiao C, Wang Z, Chen X, Yu B, Hu Y. Irradiation crosslinking and halogen-free flame retardation of EVA using hydrotalcite and red phosphorus. Radiat Phys Chem. 2006;75:557–63.

9. Lai X, Zeng X, Li H, Liao F, Yin H. Preparation and properties of flame retardant polypropylene with an intumescent system encapsulated by thermoplastic polyurethane. J Macromol Sci. 2012;51:35–47.

10. Zhang Q, Xing H, Sun C, Xiang H, Jiang D, Qin L. The mechanical properties and thermal performances of polypropylene with a novel intumescent flame retardant. J Appl Polym Sci. 2010;115:2170–7.

11. Mahmood N, Khan A, Stöckelhuber K, Das A, Jehnichen D, Heinrich G. Carbon nanotubes-filled thermoplastic polyurethane–urea and carboxylated acrylonitrile butadiene rubber blend nanocomposites. J Appl Polym Sci. 2014;131:169–72.

12. Valentini M, Piana F, Pionteck J, Lamastra F, Nanni F. Electromagnetic properties and performance of exfoliated graphite (EG)—thermoplastic polyurethane (TPU) nanocomposites at microwaves. Compos Sci Technol. 2015;114:26–33.

13. Sobha A, Narayanankutty S. Improved strain sensing property of functionalised multiwalled carbon nanotube/polyaniline composites in TPU matrix. Sens Actuators A. 2015;233:98–107.

14. Serge B, Verhart D, Gilman J, Awad W, Davis R, Morgan A, Wilkie C. Investigation of nanodispersion in polystyrene–montmorillonite nanocomposites by solid-state NMR. J Polym Sci. 2003;41:3188–213.

15. Lin M, Li B, Li Q, Li S, Zhang S. Synergistic effect of metal oxides on the flame retardancy and thermal degradation of novel intumescent flame-retardant thermoplastic polyurethanes. J Appl Polym Sci. 2011;121:1951–60.

16. Tidjani A, Wilkie C. Photo-oxidation of polymeric-inorganic nanocomposites: chemical, thermal stability and fire retardancy investigations. Polym Degrad Stab. 2001;74:33–7.

17. El-Fattah M, ElSaeed A, Dardir M, El-Sockary M. Studying the effect of organo-modified nanoclay loading on the thermal stability, flame retardant, anti-corrosive and mechanical properties of polyurethane nanocomposite for surface coating. Prog Org Coat. 2015;89:212–9.

18. Dalai S, Vijayalakshmi S, Shrivastava P, Sivam S, Sharma P. Preparation and characterization of hollow glass microspheres (HGMs) for hydrogen storage using urea as a blowing agent. Microelectron Eng. 2014;126:65–70.

19. Liu L, Hu J, Zhuo J, Jiao C, Chen X, Li S. Synergistic flame retardant effects between hollow glass microspheres and magnesium hydroxide in ethylene-vinyl acetate composites. Polym Degrad Stab. 2014;104:87–94.

20. Chen X, Jiang Y, Jiao C. Synergistic effects between hollow glass microsphere and ammonium polyphosphate on flame-retardant thermoplastic polyurethane. J Therm Anal Calorim. 2014;117:857–66.

21. Li H, Hu Z, Zhang S, Gu X, Wang H, Jiang P, Zhao Q. Effects of titanium dioxide on the flammability and char formation of water-based coatings containing intumescent flame retardants. Prog Org Coat. 2015;78:318–24.

22. Jiang W, Joens J, Dionysiou D, O'Shea K. Optimization of photocatalytic performance of TiO2 coated glass microspheres using response surface methodology and the application for degradation of dimethyl phthalate. J Photochem Photobiol. 2013;262:7–13.

23. Fateh T, Rogaume T, Luche J, Richard F, Jabouille F. Characterization of the thermal decomposition of two kinds of plywood with a cone calorimeter–FTIR apparatus. J Anal Appl Pyrolysis. 2014;107:87–100.

24. Peng H, Zhou Q, Wang D, Chen L, Wang Y. A novel charring agent containing caged bicyclic phosphate and its application in intumescent flame retardant polypropylene systems. J Ind Eng Chem. 2008;14:589–95.

25. Bocz K, Toldy A, Kmetty Á, Bárány T, Igricz T, Marosi G. Development of flame retarded self-reinforced composites from automotive shredder plastic waste. Polym Degrad Stab. 2012;97:221–7.

26. Chen X, Jiang Y, Jiao C. Smoke suppression properties of ferrite yellow on flame retardant thermoplastic polyurethane based on ammonium polyphosphate. J Therm Anal Calorim. 2014;120:1493–501.

27. Lu C, Meng D, Yu M. Study on material parameters effects on smoldering and transition from smoldering to flaming combustion. Adv Mater Res. 2011;261:571–5.

28. Ricciardi M, Antonucci V, Zarrelli M, Giordano M. Fire behavior and smoke emission of phosphate-based inorganic fire-retarded polyester resin. Fire Mater. 2012;36:203–15.

29. Marney D, Russell L, Mann R. Fire performance of wood (*Pinus radiata*) treated with fire retardants and a wood preservative. Fire Mater. 2008;32:357–70.

30. Zhao L. Novel tough and thermally stable cyanate ester resins with high flame retardancy, low dielectric loss and constant based on a phenolphthalein type polyarylether sulfone. Rsc Adv. 2015;5:58989–9002.

31. Xu T, Huang X. A TG-FTIR investigation into smoke suppression mechanism of magnesium hydroxide in asphalt combustion process. J Anal Appl Pyrolysis. 2010;87:217–23.